Prepublished Copy

NATURE ENVIRONMENT AND POLLUTION TECHNOLOGY

Article In Press

PEER-REVIEWED PREPUBLISHED MANUSCRIPT

This is a peer-reviewed prepublished version of the paper to be published in **Vol. 26, No. 1, March 2027.**

Monitoring the Spatio-Temporal Concentrations of Black Carbon Aerosols Over Iraq During 1980-2022

Baidaa J. Hassan, Yaseen K. Al-Timimi and Basim I. Wahab

RECEIVED
22 May 2026

CITE THIS ARTICLE
Hassan, B.J., Al-Timimi, Y.K. and Wahab, B.I., 2027. Monitoring the Spatio-Temporal Concentrations of Black Carbon Aerosols Over Iraq During 1980-2022. *Nature Environment and Pollution Technology*, 26(1), D1950.

https://doi.org/10.46488/NEPT.2027.v26i01.D1950

EARLY-ACCESS STATEMENT

This manuscript, after peer review, is being released online in its original, unedited form to provide early access to its findings. Prior to final publication, it will undergo additional editing and formatting. Readers may note that, as an unedited version, the manuscript may have linguistic and other minor errors. The DOI will be active after the final publication of the paper.

PUBLICATION STATUS

PEER REVIEW	ONLINE VERSION	FINAL ISSUE
Completed	Prepublished	March 2027

© The Author(s) 2027. This article is Open Access under the Creative Commons Attribution 4.0 International License, allowing use, sharing, adaptation and reproduction with proper credit. Images or third-party material are covered by this licence unless otherwise noted. For uses beyond the licence, permission must be obtained from the copyright holder. Licence details: creativecommons.org/licenses/by/4.0/.

Monitoring the Spatio-Temporal Concentrations of Black Carbon Aerosols Over Iraq During 1980-2022

Baidaa J. Hassan[1†], Yaseen K. Al-Timimi[2], Basim I. Wahab[3]

1 Department of Atmospheric Sciences, College of Science, Mustansiriyah University, Baghdad, Iraq.

2 Department of Atmospheric Sciences, College of Science, Mustansiriyah University, Baghdad, Iraq.

3 Department of Atmospheric Sciences, College of Science, Mustansiriyah University, Baghdad, Iraq.

† Corresponding author: Baidaa J. Hassan; baidaa71.atmsc@uomustansiriyah.edu.iq

https://orcid.org/0000-0001-5608-5734

Abstract

Black Carbon (BC) concentration has a significant impact on the climate, environment, and human health. In the Middle East, rapid urbanization, outdated vehicles, outdated air quality standards, and decaying infrastructure contribute to poor air quality. MERRA-2 reanalysis data of BC were used in this research to monitor the annual, seasonal, and monthly spatial distributions of BC concentrations in Iraq. This study examines the temporal and spatial distribution pattern of black carbon (BC) concentrations in Iraq during 1980–2022. The Mann–Kendall test was used to detect trends in BC monthly, seasonal, and annual data. The analysis shows a statistically significant positive trend ($p < 0.05$) for all months and seasons. The highest mean monthly slope magnitudes were in November, December, and January ($Q = 0.012$ μg m^{-3} $year^{-1}$), while the lowest occurred in May, June, and July ($Q = 0.0054–0.0058$ μg m^{-3} $year^{-1}$). The annual change in BC concentration was 0.34 μg m^{-3}, and the highest increase (0.51 μg m^{-3}) occurred in November and December. On a seasonal basis, the increase was strongest in winter ($Q = 0.0117$ μg m^{-3} $year^{-1}$), followed by autumn and spring, with summer displaying the weakest trend of all seasons. Spatially, the central and southern regions of Iraq had consistently high BC concentrations (greater than 1.8 μg m^{-3} in winter), compared with lower concentrations on the order of 0.2–1.0 μg m^{-3} in the northern and western areas. The central region came first, followed by the southern, northern, and western regions. Seasonal fluctuations were significant: the most polluted seasons were winter and autumn, due to heavy fuel combustion for building heating, which creates calm atmospheric conditions with high humidity. In summer, concentrations were lower due to deep convective mixing driven by a deeper turbulent planetary boundary layer, leading to greater dispersion. The spatial gradient persisted across all seasons, pinpointing the focal southern urban-modern belt as a persistent contamination hotspot. The results thus underpin mitigation strategies to reduce combustion emissions from domestic heating, diesel generators, and other anthropogenic sources.

Keywords: Air pollution, Black carbon, Iraq, GIS, IDW, Mann-Kendall

Introduction

Black Carbon (BC), commonly referred to as soot, is a significant air pollutant composed of fine dark particulate matter ($PM_{2.5}$) containing carbon-rich particles generated from the incomplete combustion of biofuels, fossil fuels, and biomass (Kouassi, 2021; Ahmed et al., 2014). During the Industrial Revolution, the combustion of biological and agricultural waste, human usage of oils, coal, and more fossil fuels, as well as exhaust emissions from vehicles, have all led to an abrupt rise in the atmospheric concentration of BC aerosols. (Zhang and Wang, 2011). Aerosols are tiny solid or liquid particles suspended above the ground that result from anthropogenic and natural processes (Samudro et al., 2023). The evaluation of aerosols' role in radiative forcing and, consequently, climate change is fraught with ambiguity due to the geographical and temporal variability in their physical and chemical properties (IPCC, 2013). Black Carbon has emerged as a key driver of changes in atmospheric thermodynamics and of the warming of the region's atmosphere associated with those changes and shifts in precipitation patterns (Davuliene et al., 2019). A significant constraint and source of uncertainty in climate models is the lack of systematic, long-term chemical and physical aerosol data from sites that represent diverse ecosystems (Raju et al.,2016). Aerosols containing black carbon have a substantial influence on the climate system through various mechanisms, including direct absorption of solar radiation (Bond et al., 2013). Modifying the surface albedo affects cloud characteristics, thermal stability, circulation, and precipitation (Lund et al., 2017). After its deposition, it lowers the albedo of ice and snow cover (Zhang et al.,2019). Reducing emissions in BC can help improve air quality in some countries, such as China (Ding et al., 2016). Additionally, it can greatly alleviate global warming (Grieshop et al., 2009; Samset et al., 2013). Since small-scale laboratory research and sparse field observations are the primary sources of emission factors, estimates of gas-flaring BC emission factors vary widely (CAPP, 2007; Amann et al., 2011). Different sources of BC can be significant. Home combustion is the main source, along with on-road transportation and on-road diesel vehicles (Subramanian et al., 2016; Conrad & Johnson, 2017). More concentrated black carbon is typically observed in winter due to increased energy use, unfavorable weather, and the sporadic but significant influence of combustion in particular locations during summer and spring (Becerril et al., 2017; Bian et al., 2018; Hyvärinen et al., 2011). Basim and others studied the correlation between Black Carbon (BC) concentrations and meteorological factors in Iraq using long-term data from 1980 to 2022. They analyzed spatial variation with the Pearson correlation coefficient (Wahab et al., 2023). In recent years, air quality has been a major factor in shaping urban quality of life, particularly in industrial and densely populated areas. Human health is impacted by a range of air pollution-related effects, including dermal, respiratory, Alzheimer's disease, stroke, lung disease, and asthma, in addition to mortality and cardiovascular effects. There are many studies on BC and its effects on human health and climate change in Middle Eastern countries and the ambient regions (Chen et al., 2022). Air pollution particles remain a significant issue in Makkah. There were significant temporal variabilities in $PM_{2.5}$ levels (Nayebare et al., 2018). This research aims to examine the spatial and temporal distributions of monthly, seasonal, and annual black carbon values in selected areas of Iraq, representing the northern, middle, and southern regions (Al-Jeelani, 2009).

Materials and Methods

Area of Study

Iraq is a Middle Eastern country. (the Asian continent's western south) The northern border is with Turkey. Saudi Arabia is to the south, Jordan and Syria to the west, Iran to the east, and Kuwait to the southeast. Its approximate coordinates are 33.2°N, 43.5°E (Al-Lami et al.,2021). Subtropical high pressure has a significant impact on Iraq's summer climate. Periodic low-pressure systems replace the subtropical high-pressure system that moves from west to east through Iraq, delivering winter showers and snow north into the mountain ranges. The high-temperature extremes within a single day and between the winter and summer seasons are among Iraq's most notable characteristics (Sadar et al., 2023; Zangana et al., 2021). Iraq is located in the moderate northern region, which has a rainfall pattern similar to the Mediterranean, with rainfall occurring almost exclusively in autumn, spring, and winter, and not in summer. Based on annual rainfall amounts, the region is usually divided into northern, middle, and southern rainy zones. The northeast and northern Iraq typically receive more rain than the south. Iraq's northern region has lower wind speeds than its central and southern regions, and, based on seasonal wind speeds, the highest values were recorded in summer and spring. In contrast, the lowest were recorded in fall and winter (Muter et al., 2024). The surface of Iraq is classified into four major parts: Mountainous Area: It accounts for approximately 5 % of the overall area, with the majority located in the northern and northeastern parts of the country. This region of Iraq is considered the most important for its water sources. Hills and Plateau Regions: This region comprises 15 % of Iraq's total land area (approximately 200-1000 meters above sea level). Alluvial Plain Region: Located in central and southern Iraq between the Tigris River and the Euphrates River (30% of the entire Iraqi area). It is a flat, fertile plain composed of river sediments and is considered the main agricultural area in Iraq. The Desert Region: It covers western and southwestern Iraq (50%). This region is mostly dry and includes rocky deserts, sandy areas, and sparse vegetation (Adeeb & Al-Timimi, 2019).

Gridded Concentrations

This study used Black Carbon Surface Mass Concentration (M2TMNXAER v 5.12.4) in Iraq over the period from 1980 to 2022 (504 months). The datasets are monthly time-averaged data from the Modern-Era Retrospective Analysis for Research and Applications version 2 (MERRA-2). This is a collection of aerosol types assimilated diagnostics: (column mass density of aerosol components; black carbon, dust, sea salt, sulfate and organic carbon). MERRA-2 is the latest version of global atmospheric reanalysis for the satellite era produced by the NASA Global Modeling and Assimilation Office (GMAO) using the Goddard Earth Observing System Model (GEOS) version 5.12.4. The variable used within this study is black carbon surface mass concentration ($\mu g\ m^{-3}$), which equates to the modelled near-surface mass concentration of black carbon aerosol particles. Values are reported at surface level (model layer closest to the surface): they are NOT column-integrated aerosol optical depth or total column burden .The data were downloaded from the NASA Goddard Earth Sciences Data and Information Services Center (GES DISC) via the following link: https://disc.gsfc.nasa.gov/datasets/M2TMNXAER_5.12.4/summary. The dataset provides global horizontal coverage with a spatial resolution of 0.5° latitude × 0.625° longitude. The data are provided as gridded fields with a horizontal resolution of 0.5° × 0.625° (latitude × longitude), covering the global domain. The number of grid cells within Iraq after clipping was 137, which were extracted based on the country's administrative boundaries. All grid distributions are shown in Figure 1 for the period 1980–2022.

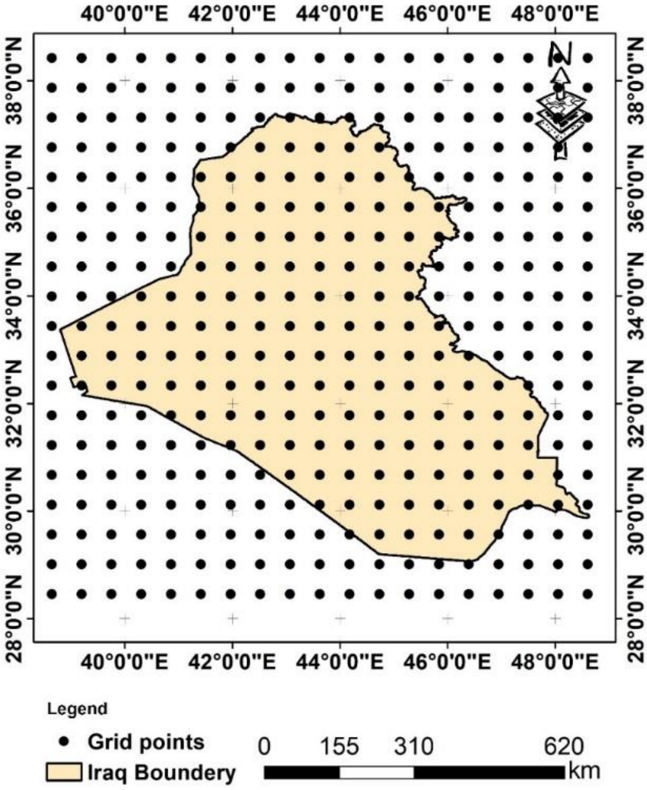

Figure 1. The study area of Iraq.

MERRA-2 BC column concentrations have shown correlations of R = 0.60–0.85 against AERONET-derived retrievals (Zhang et al., 2024). Nevertheless, we acknowledge that reanalysis products are subject to regional biases, particularly in data-sparse regions like Iraq, where ground-based measurements remain limited. Such biases, however, tend to be systematic and do not substantially affect the detection of long-term trends, which is the primary focus of this study. Future work incorporating local measurements would further refine the absolute concentration estimates.

Methodology

The spatial distribution of monthly concentrations of BC was carried out using the Geographic Information System (GIS technique. An accurate graphical depiction of features in space can be created using computer-based tools called Geographic Information Systems (GIS), which include capabilities for data collection, integration, analysis, modeling, management, and presentation (Hassan, 2018). ArcGIS is the most widely used application developed by the Environmental Systems Research Institute (ESRI), with an easy-to-use graphical interface, the ability to handle multiple types of geographic objects, and a collection of robust extensions and tools (Sánka, 2015).

The calculation of property amounts at unnamed sites within the area covered by the current observation sites is known as spatial interpolation. In most cases, spatial interpolation procedures are performed using GIS. Different strategies for classifying spatial interpolation methods include exact and approximate interpolation, point and area interpolation, global and local, and many others. Numerous systems exist for interpolating both locally and globally; Fourier series and trend surface analysis are two instances of global systems, whereas proximal interpolation, Kriging, the B-spline approach, and Inverse Distance Weighting (IDW) are popular GIS spatial interpolation techniques. It is used to estimate unknown values at specific locations using known values from surrounding measurement points. (It weights data only by distance from the interpolation site, using data from neighboring places to make predictions) (Huang et al., 2011). Aside from the essential premise, the locations of the interpolation's proximal points should be weighted more heavily than those of distant points. Regarding spatial linkages, IDW makes no assumptions.

IDW is extensively used with MERRA-2 reanalysis data. Recent studies have successfully applied IDW to visualize and analyze MERRA-2 reanalysis products for air quality and climate applications in the Middle East region. For instance, (Liu et al., 2025) downscaling studies of MERRA-2 $PM_{2.5}$ data over the Arabian Gulf and Persian Gulf regions have employed IDW alongside other interpolation methods to generate continuous spatial surfaces.

IDW is widely recognized as an effective visualization tool for spatial data. The method produces continuous surfaces that facilitate the identification of spatial patterns and gradients, which are often difficult to discern from discrete grid cells alone. As noted by (Atta, 2020), the IDW is also observed to exhibit high prediction accuracy, and IDW interpolation does not distort the spatial distribution.

Cell values are computed using this method, based on a collection of linearly weighted sample points. The opposite distance determines the weight. With IDW, the user can control the importance of known points in the given data based on their proximity to the output point (Hessl et al.,2007). IDW is primarily predicated on two theories. First, compared to remote control points. Proximity control points have a more significant impact on the interpolated value of a point. The inverse separation between the force-raised points directly corresponds to the degree of impact (weight) of the points (Huang et al., 2011). Inverse Distance Weighting requires certain trigger parameters, such as the homogeneity factor, the exponential factor, and the search neighborhood parameters. It works particularly well with small data sets, where traditional interpolation techniques could have problems. This method is quite flexible and can be used to evaluate the data set in terms of information flow or contrast within the study topic (Garnero & Godone, 2014). The equation defines inverse-distance interpolation.

$$Z = \frac{\sum_{i=1}^{k} W_{ij} Z_i}{\sum_{i=1}^{k} W_{ij}} \quad (1)$$

Zi is the observed value at the point of control I (i = 1, ..., k); Z is the approximate point to be found, where Wi is the weighting function that determines, during the interpolation process, each control point's relative importance Zi. K points are utilized in total for the interpolation process. This weighting relationship means that data points near the interpolation point receive relatively large weights, whereas those farther away receive relatively small weights (Robinson & Metternicht, 2003). The following equation was used to determine the arithmetic mean of BC concentration (Reimann et al.,2011):

$$\overline{BC} = \frac{1}{n} \sum_{i=1}^{n} (BC)_i \quad (2)$$

N: shows the total number of points within the region under study, whereas the mean is indicated by ($^{-}$).The standard deviation (SD): This characterizes the data's average distribution around the core value. Moreover, it can be computed using the following equation:

$$\mathrm{SD} = \sqrt{\frac{1}{n-1} \sum_{i=1}^{n} (x_i - \bar{x})^2} \quad (3)$$

The temporal distribution of monthly concentrations of BC was carried out by the Mann-Kendall test. For the computation of this statistical test, MAKESENS was used. It was specifically designed to detect and estimate trends in time series of annual environmental and atmospheric data (such as precipitation chemistry, temperature, or air pollutants like black carbon), a brief version of the Mann-Kendall test and Sen's method exploits both the S statistics and the normal-approximation Z statistics, as in Gilbert (1987). For time series with fewer than 10 data points, the S test is used; for those with 10 or more, the normal approximation is used.

Trends were detected in the time series using the Mann-Kendall test. The World Meteorological Organization has recommended the Mann-Kendall method for assessing trends in environmental time series.

The Mann-Kendall test statistic S is given by:

$$S = \sum_{k=1}^{n-1} \sum_{j=k+1}^{n} sgn(xj - xk) \quad (4)$$

X_i and x_k are the annual values in years' j and k, j>k, respectively, and

$$sgn(xi - xj) = \begin{cases} 1 & if \ xi - xj > 0 \\ 0 & if \ xi - xj = 0 \\ -1 & if \ xi - xj < 0 \end{cases} \quad (5)$$

When n is nine or lower, the absolute value of S matches the theoretical distribution of S obtained by Mann-Kendall (Gilbert, 1987). The Z-statistic is used when the number of values is 10 or more. When n is at a minimum of 10, the normal approximation test is applied. Although there are various tied values, for example, similar values in the time series, this may decrease the veracity of the normal distribution when the number of values is near ten. The contrast of S calculated by equation (4), with consideration that ties would be displayed as:

$$VAR = \frac{1}{18}\left[n(n-1)(2n+5) - \sum_{p=1}^{q} tp\ (tp-1)(2tp+5)\right] \quad (6)$$

q is the number of tied groups.

tp is the number of data values in the pth group.

The values of S and VAR(S) are used to calculate the Z-test as follows.

$$Z = \begin{cases} \frac{S-1}{\sqrt{VAR(S)}} & if \ S > 0 \\ 0 & if \ S = 0 \\ \frac{S+1}{\sqrt{VAR(S)}} & if \ S < 0 \end{cases} \quad (7)$$

The presence of a statistically significant trend is estimated using the Z-value. A positive (negative) value of Z indicates an upward (downward) trend (Gilbert, 1987).

The Mann–Kendall (MK) test, in conjunction with Sen's slope estimator, is the most widely applied non-parametric trend analysis method in atmospheric and hydrological research. While the MK test theoretically requires serially uncorrelated time series, the choice of whether and how to correct for autocorrelation is not straightforward. (Collaud Coen et al. 2020b) systematically evaluated the effects of various pre-whitening methods on MK trend detection using multiple in situ aerosol time series and demonstrated that the selection of pre-whitening procedure has direct consequences for the statistical significance, the estimated slope value, and the confidence limits. Importantly, pre-whitening does not universally improve trend identification; it may weaken the true trend magnitude and, in some cases, produce erroneous results. Given that our dataset comprises 504 monthly observations spanning 43 years (1980–2022), a length substantially exceeding the typical 10- to 40-year series examined in aerosol trend studies, the statistical power is sufficient to detect robust trends even in the presence of moderate autocorrelation. Furthermore, the consistency of the positive trends across all months and seasons ($p < 0.05$ for all 12 months), combined with coherent spatial patterns that align with known emission sources and meteorological drivers, provides strong independent evidence that the detected signals are real and not artifacts of serial correlation.

Results and discussion.

Temporal distribution of BC concentrations

The Mann–Kendall test was used to identify the pattern for the analysis of monthly, seasonal, and annual concentrations of BC. The monthly concentrations of BC and their standard deviations for the period from January to December are shown in Figures 2 and 3. The analysis of BC concentrations during the first half of the year reveals a distinct upward trend as the region transitions from winter to early summer, and the concentrations of BC for the period from July to December show a similar trend. The analysis of BC concentrations from July through December reveals an upward trend, particularly as the region transitions from the dry summer months into the stable atmospheric conditions of late autumn and winter. This pattern results from shifts in meteorological parameters and changes in human activity.

Monthly BC concentrations in the study area show a statistically significant positive trend across all 12 months. The magnitude of slope (Q) for significant trends was (0.01, 0.009, 0.0069, 0.0064, 0.0058, 0.0055, 0.0054, 0.007, 0.008,0.0098,0.012,0.012) $\mu g\ m^{-3}\ year^{-1}$ for (Jan., Feb., Mar., Apr., May, Jun., Jul., Aug., Sep., Oct., Nov., and Dec.) respectively. The months November, December, and January show high trend values, while the months May, June, and July show the lowest trend values for mean BC concentration. The winter months are characterized by rising mean BC concentrations, with slight increases or levels nearly the same as in the Autumn months (October and September). The statistical test results reveal that all BC mean concentrations are statistically significant at the $P < 0.001$ level across all months and seasons.

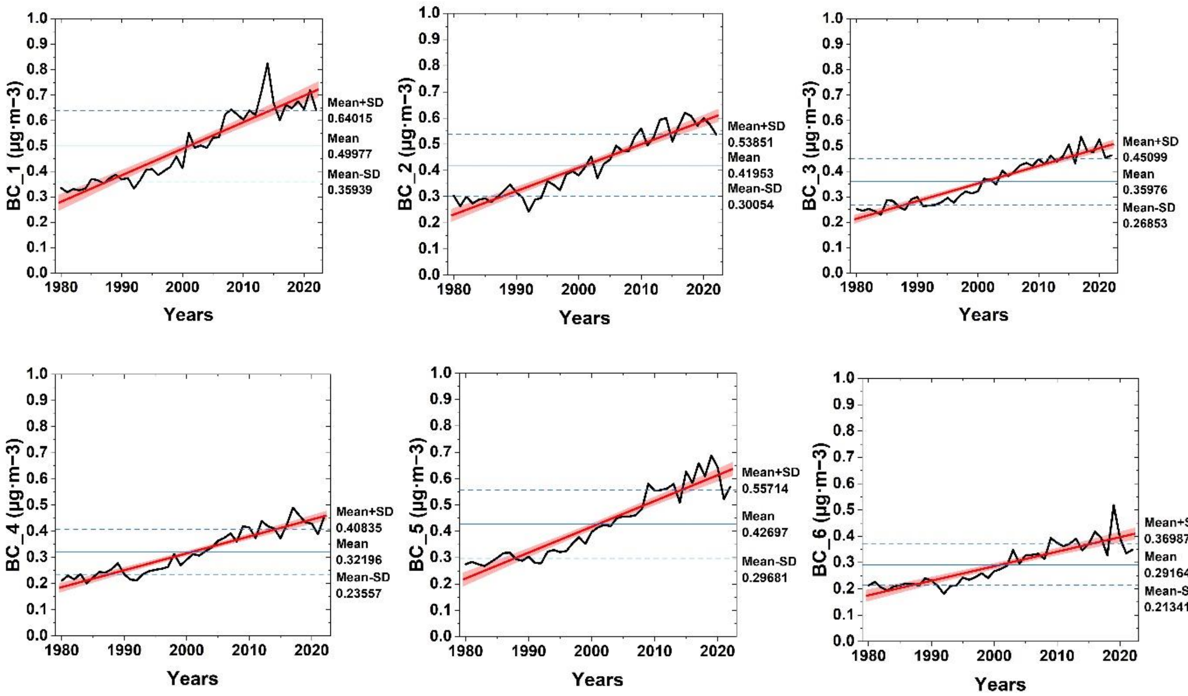

Figure 2. Monthly variation trend of black carbon concentration for January to June during the study period.

From Table 1, the results of the monthly analysis show that the highest increase in the annual increase was (0.51) µg m^{-3} noticed in November and December, and the lowest increase was (0.23) µg m^{-3} noticed in July.

The slope magnitude (Q) was estimated to detect significant trends (µg m^{-3} year $^{-1}$) across all seasons and in the annual mean concentration of BC in Iraq. Figure 4 shows the trends of the BC time series. It can be seen that there is a statistically significant positive trend during all seasons and in the annual mean.

Table 2 reports the seasonal trend characteristics in Iraq. It is clear from the Table that the seasonal trends (Winter, Spring, Summer, Autumn) of the mean seasonal BC concentration were (0.0117, 0.0074, 0.0056, 0.0083) µg m^{-3} year $^{-1,}$ respectively. The winter and Autumn represented a high value of the trend (0.47, 0.35) µg m^{-3}, while the summer represented the lowest value (0.24) µg m^{-3} of the trend of mean BC concentration.

The annual mean of BC concentration and the trend line are presented in Figure 4. The Mann–Kendall test confirmed that the observed positive trend is statistically significant; see Table 2. The mean annual BC concentration shows an increasing trend, which is statistically significant at the $P < 0.001$ level. A linear fit to the ensemble-averaged annual means confirms significant and quite large trends of 0.0082 µg m^{-3} year $^{-1}$. This trend corresponds to an increase of 0.34 µg m^{-3} in the total period analyzed (1980-2022).

Table 1. The results of the Mann-Kendall test (Q, 95% Confidence Interval, p-value, Z, and R^2) for monthly concentrations of BC (1980–2022; $n = 43$ years per month).

Month	Slope magnitude µg m^{-3} y^{-1}	Annual increase μg m^{-3}	95% Confidence Interval	p-value	Z
Jan.	0.011	0.47	(0.0066 – 0.0102)	< 0.001	7.598
Feb.	0.009	0.39	(0.0065 – 0.0099)	< 0.001	7.012
Mar.	0.0069	0.30	(0.0048 – 0.0077)	< 0.001	7.368
Apr.	0.0064	0.27	(0.0053 – 0.0082)	< 0.001	7.849
May	0.0058	0.25	(0.0071 – 0.0109)	< 0.001	7.514
Jun.	0.0055	0.24	(0.0022 – 0.0041)	< 0.001	7.954
Jul.	0.0054	0.23	(0.0026 – 0.0046)	< 0.001	6.907
Aug.	0.007	0.30	(0.0036 – 0.0060)	< 0.001	6.405
Sep.	0.008	0.34	(0.0053 – 0.0083)	< 0.001	6.803
Oct.	0.0098	0.42	(0.0087 – 0.0127)	< 0.001	7.703
Nov.	0.012	0.51	(0.0076 – 0.0115)	< 0.001	7.326
Dec.	0.012	0.51	(0.0062 – 0.0095)	< 0.001	7.012

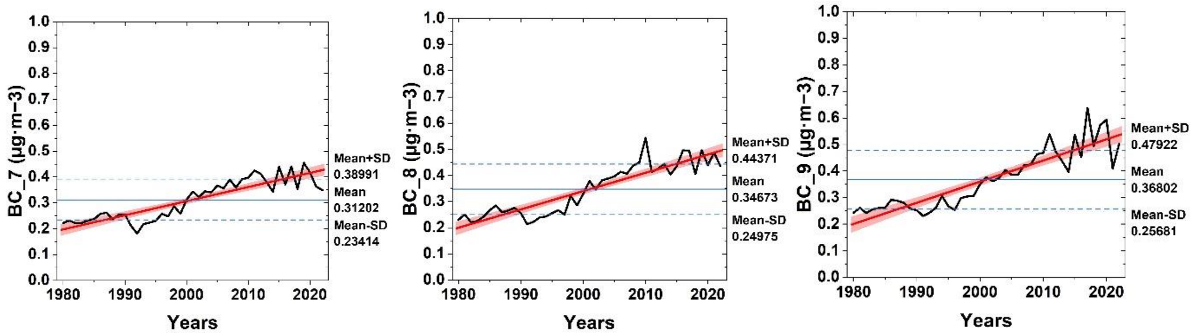

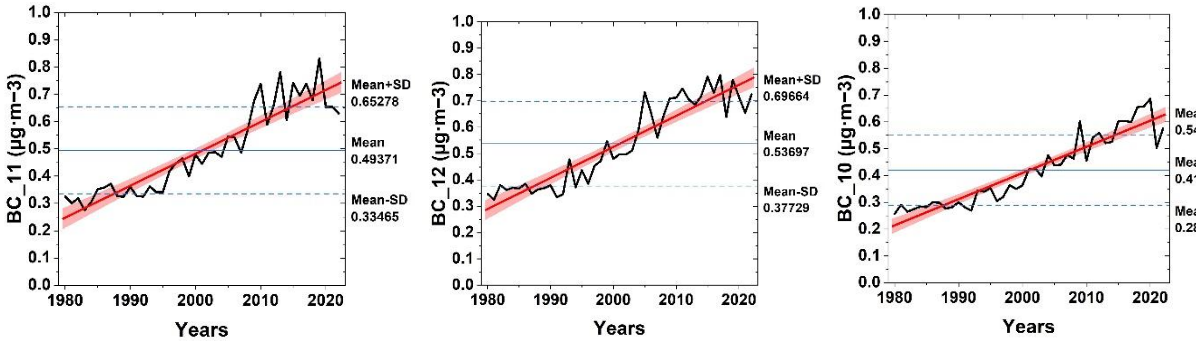

Figure 3. Monthly variation trend of black carbon concentration for July to December during the study period.

Table 2. The results of the Mann-Kendall test (Q, Q, 95% Confidence Interval, p-value, Z, and R^2) for seasonal concentrations of BC (1980–2022; $n = 43$ years per season).

Month	Slope magnitude $\mu g\ m^{-3}\ y^{-1}$	Annual increase $\mu g\ m^{-3}$	95% Confidence Interval	p-value	Z
Winter	0.0117	0.47	(0.0070, 0.0098)	< 0.001	7.31
Spring	0.0074	0.32	(0.0042, 0.0062)	< 0.001	7.41
Summer	0.0056	0.24	(0.0032, 0.0052)	< 0.001	7.46
Autumn	0.0083	0.35	(0.0062, 0.0089)	< 0.001	6.97
Annual	0.0082	0.34	(0.0051, 0.0072)	< 0.001	7.29

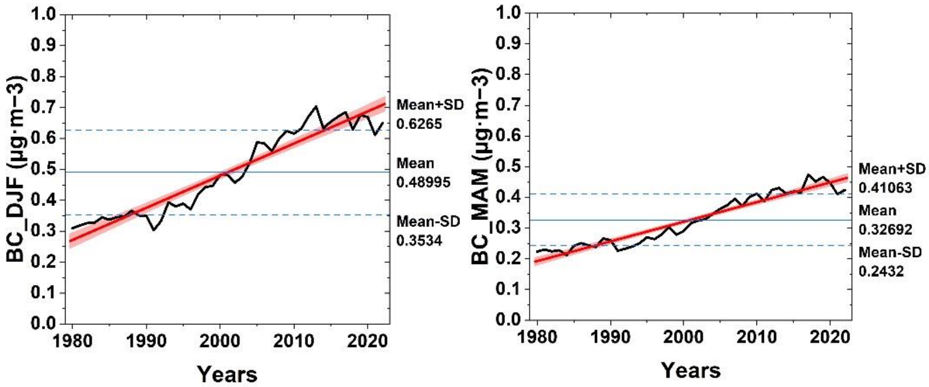

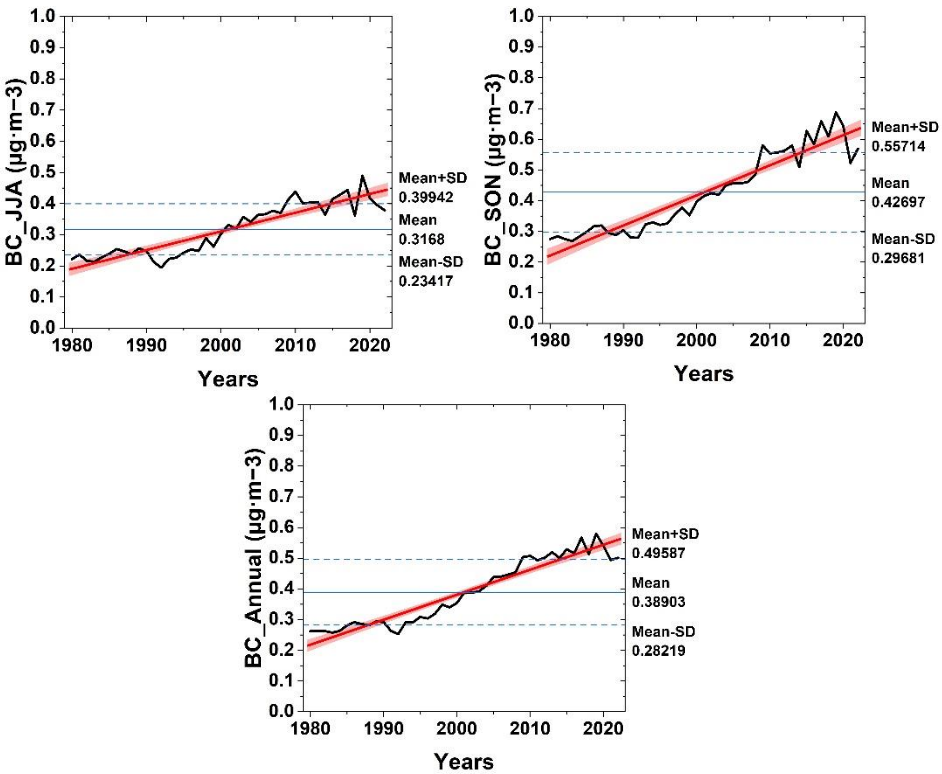

Figure 4. Seasonal and annual trend of black carbon concentration during the study period.

Spatial distribution of BC concentrations

The monthly mean concentrations of black carbon (BC) in Iraq from December to July during 1980-2022 are shown in Figure 5. In December, BC concentrations were highest in the central and southern regions, peaking above 1.8 µg m^{-3}, while the northern areas recorded lower concentrations, ranging from 0.4 to 1.0 µg m^{-3}. January saw a similar trend, with the central and southern regions again exhibiting elevated concentrations (1.4->1.8 µg m^{-3}), particularly in urban centers such as Baghdad, Nasiriya, and Basra. In contrast, the western regions showed reduced levels (0.2 to 1 µg m^{-3}).

In February, BC concentrations were mostly high again in the center and south, though they decreased compared to January, ranging from 1.2 to 1.6 µg m^{-3}, with the northern areas recording 0.8 to 1.2 µg m^{-3}. The trend continued into March, where BC levels dropped again, with the central and southern ranges at about 1.0 µg m^{-3} and the northern region at 0.4 to 0.6 µg m^{-3}.

By April, BC concentrations further declined, particularly in the central and southern areas (0.8 to 1.2 µg m^{-3}), with the northern region seeing values of 0.4 to 0.6 µg m^{-3}. In May, levels continued to decrease, with approximately 1.2 µg m^{-3} noted in the central region and lower concentrations in the western areas.

Figure 6 shows the Spatial distribution of the monthly average of BC concentrations in Iraq from June to November. June saw a notable decline in BC levels across Iraq, with central and southern areas ranging from 0.4 to 0.8 µg m^{-3}. The western region had quite low concentrations (0.2 to 0.4 µg m^{-3}), while the northern areas were between 0.4 and 0.6 µg m^{-3}. The trends reversed in July, when concentrations increased again, especially in the southern and central regions, where levels ranged from 0.6 to 1.0 µg m^{-3}, peaking at 1.2 µg m^{-3} in the core of the central region, while the western and northern areas reported milder increases (0.2 to 0.8 µg m^{-3}). This analysis elucidates the significant seasonal variability of BC concentrations across Iraq.

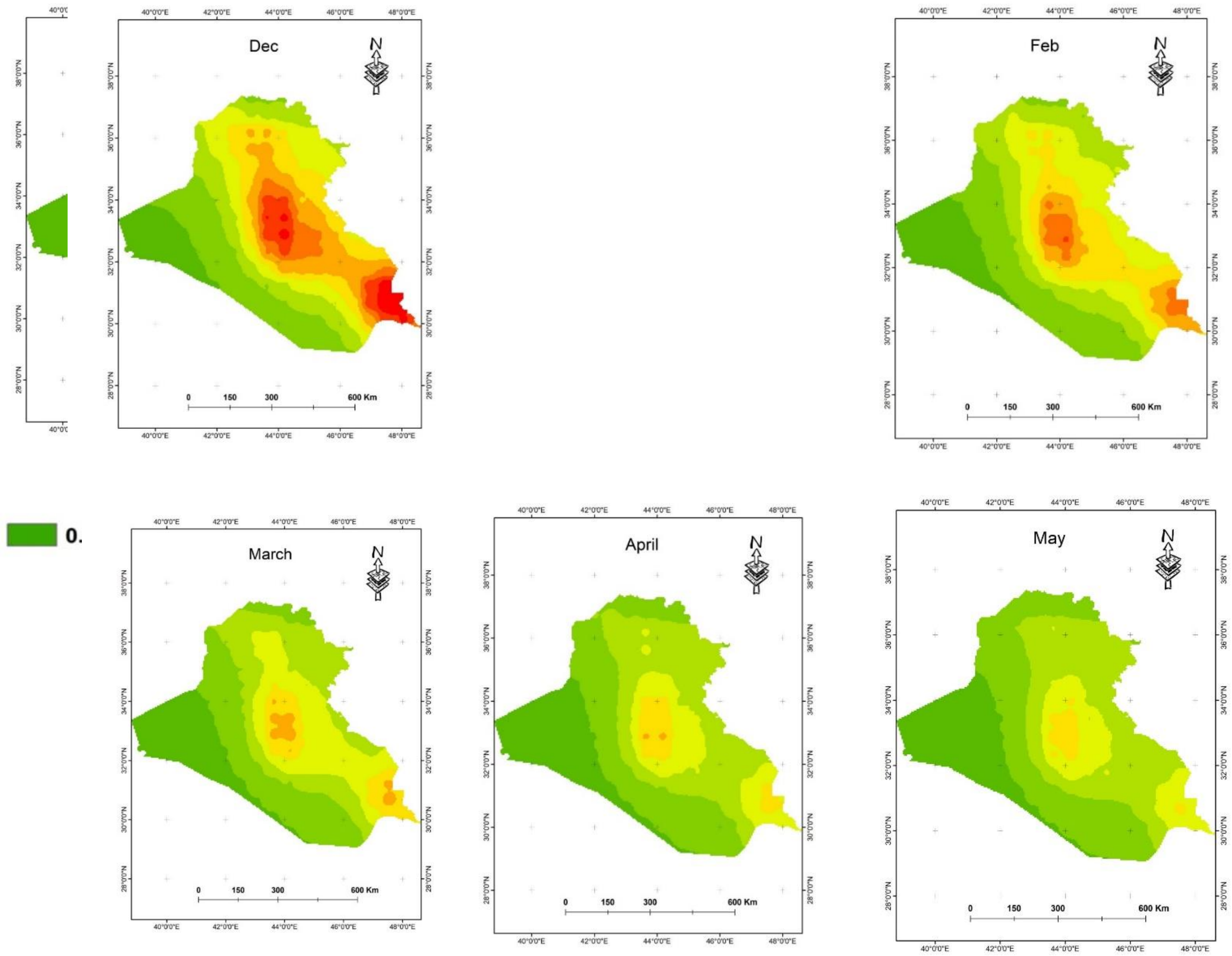

Figure 5. Spatial Distribution of the monthly mean of BC concentrations in Iraq from December to May.

The highest BC concentrations were observed in winter (Figure 7), followed by autumn, spring, and summer, with the lowest in summer. During the winter months of December, January, and February, BC concentrations fluctuate between high values. If you look at the monthly values, you can see that the highest levels were in December, followed by January and February. Figure 7, which depicts high BC concentrations, reflects this, as the central and southern regions recorded higher BC concentrations than in other seasons, ranging from 1.4 to 1.8 µg m^{-3}. Moreover, in the southern area and the central region, values exceeding 1.8 µg m^{-3} may be attributable to high relative humidity at this time of year. BC concentration rates were measured in the northern region at 0.8 1.4 µg m^{-3}, followed by the western region at 0.4 - 0.6 µg m^{-3}.

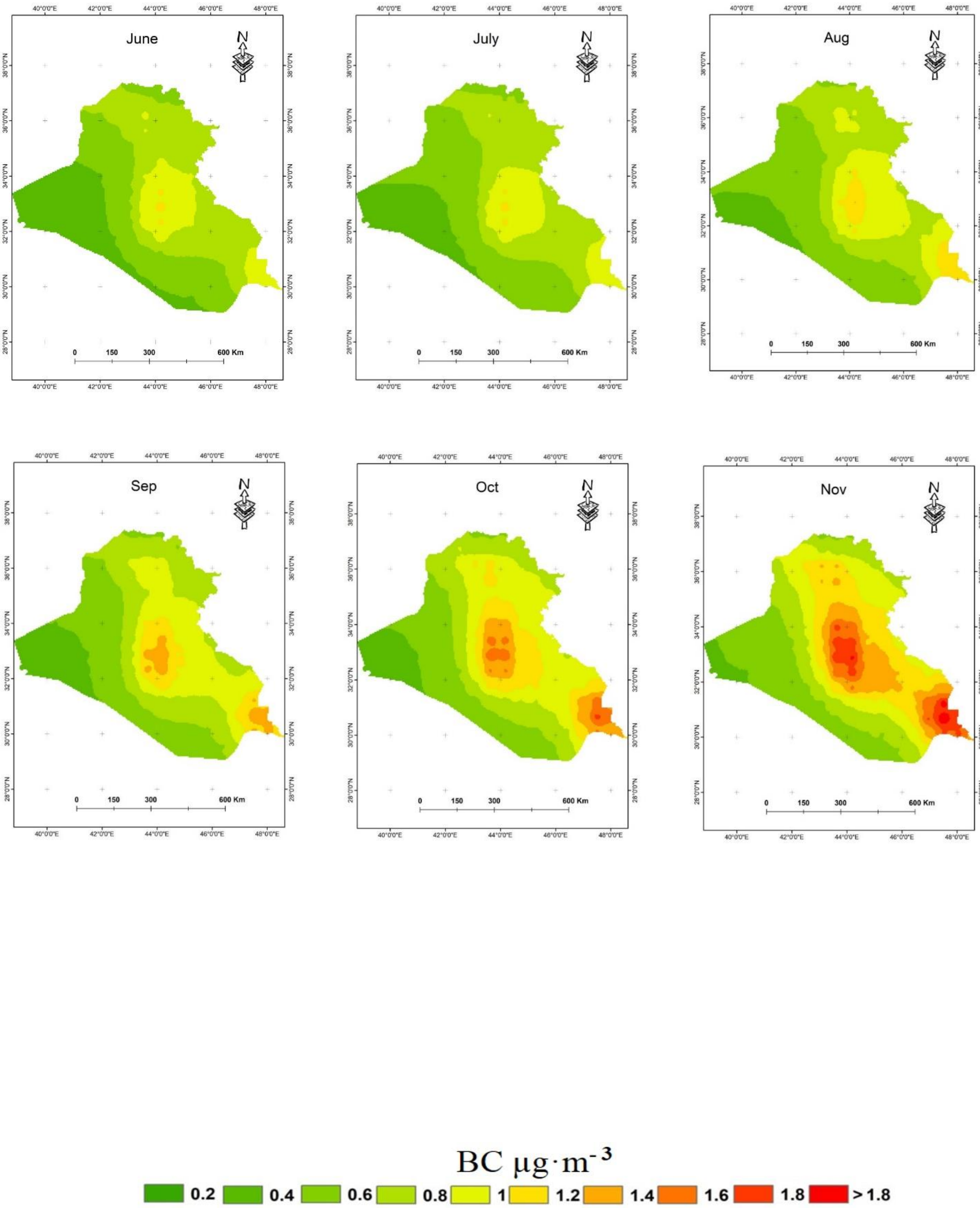

Figure 6. Spatial Distribution of the monthly average of BC concentrations in Iraq from June to November.

By examining the Spring months of April and March, we notice a clear and effective decrease in BC concentration rates, with similar behavior. The BC concentration rates in the central and southern areas are the highest, ranging from 0.8 to 1.2 µg m^{-3} and up to 1.6 µg m^{-3} in the core of the central region. Next comes the northern region, where concentrations range from 0.8 to 1.0 µg m^{-3}, and then the western region, where levels range from 0.2 to 0.4 µg m^{-3}. The pollutant concentration values during the study period were lowest in the summer months of June, July, and August. The distribution of BC concentration rates was similar, with the central region recording the highest value during this season, between 0.6 and 1.0 µg m^{-3}, centered around 1.2 µg m^{-3}; the southern region between 0.8 and 1.0 µg m^{-3}; and the Southeast around 1.2 µg m^{-3}. BC concentrations in the northern and western regions, respectively, range from 0.4 to 0.8 µg m^{-3} and 0.4 to 0.6 µg m^{-3}. After the winter season, the fall season, represented by September, October, and November, had the second-highest BC concentration rates. The highest values ranged from 1.0 to 1.8 µg m^{-3} in the central and southern sections and were slightly above 1.8 µg m^{-3} in the southeast core. The northern region had BC concentration rates between 0.8 and 1.2 µg m^{-3}, whereas the western region had values between 0.2 and 0.6 µg m^{-3}. One of the causes of the high concentrations of BC in the winter and autumn months may be atmospheric humidity.

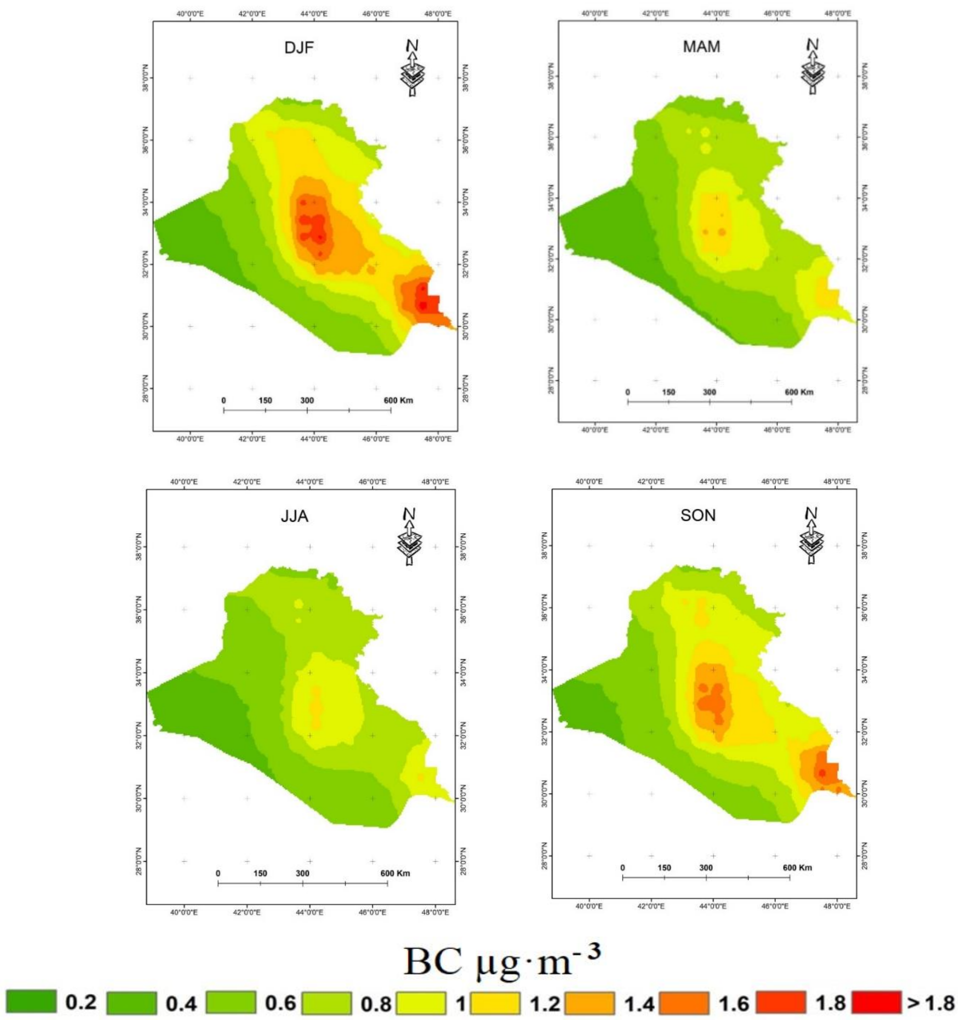

Figure 7. Spatial distribution of the seasonal average of Black Carbon concentrations in Iraq.

From Figure 8, it is possible to observe the behavior of BC concentration values as follows: Following the central region, which recorded the highest concentration values between 0.8 and 1.2 µg m^{-3} but is lower than it was in the winter and autumn seasons, were the southern and southeastern regions, which recorded concentration values between 0.6 and 1.0 µg m^{-3}. Then came the northern region, which had concentration values ranging from 0.4 to 0.6 µg m^{-3}. The lowest concentrations in the study area were observed in the western region, ranging from 0.2 to 0.4 µg m^{-3}. A summary of the BC concentration rate behavior clearly shows that the central region recorded higher values than the southern, northern, and western sectors.

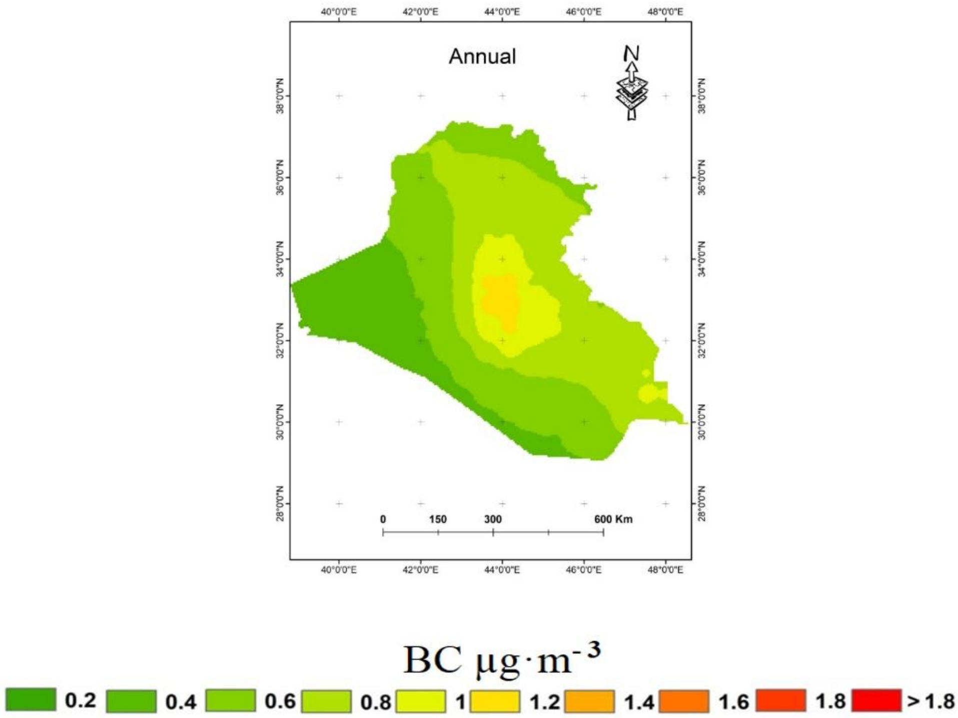

Figure 8. Spatial distribution of the annual average of Black Carbon concentrations in Iraq.

Figure 9 (A and B) shows the monthly and seasonal distribution of BC concentrations. The monthly distribution reveals that BC concentrations peak in the winter months (December and January), followed by a secondary peak in late autumn (November). The cold season necessitates increased fuel consumption for domestic heating and the localized use of diesel generators, both of which are primary sources of black carbon (BC) emissions. A gradual decline is observed as we move into April and May. This is likely due to the increase in the Planetary Boundary Layer (PBL) height and enhanced thermal convection, which facilitates the dilution and dispersion of aerosols. (The Planetary Boundary Layer (PBL), also known as the atmospheric boundary layer, is the lowest part of the atmosphere that is directly influenced by its contact with the Earth's surface).

The Winter season emerges as the most polluted season. The combination of stagnant air and high emission density leads to maximum BC accumulation. In Summer, despite high temperatures and potential increases in electricity-related emissions (cooling), the concentrations are often lower than in winter. This is attributed to high wind speeds and unstable atmospheric conditions, which promote both horizontal and vertical transport. The autumn season shows a rising trend, potentially linked to the onset of atmospheric stability and to agricultural biomass burning activities that often occur post-harvest.

Figure 4 shows High and Low in Winter and (Spring/Summer) respectively. The larger standard deviations in January and December suggest that BC levels are highly susceptible to episodic spikes. These could be "heavy pollution days" triggered by specific weather events or localized intense burning.

Low SD in Spring/Summer suggests a more uniform and stable emission profile, representing a consistent urban "background" concentration with fewer extreme fluctuations.

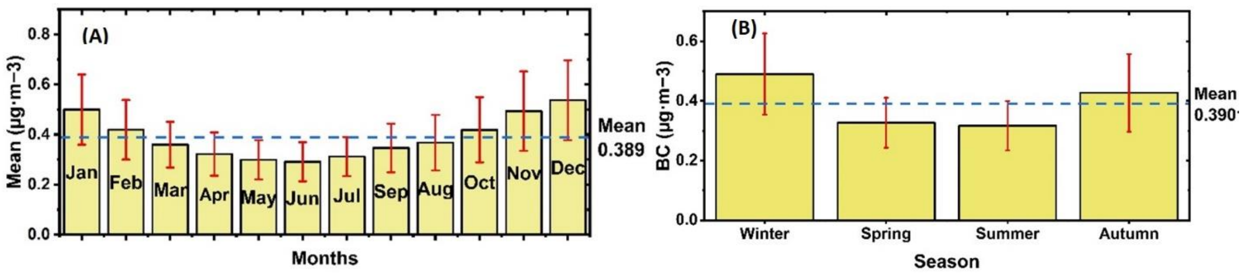

Figure 9. Monthly and seasonal variation in black carbon concentration during the study period.

Conclusions

The temporal analysis of BC concentrations over the study period reveals a statistically significant ($p < 0.001$) positive trend for all months and seasons. Monthly slope magnitudes varied from 0.0054 µg m^{-3} $year^{-1}$ (July) to 0.012 µg m^{-3} $year^{-1}$ (November and December); the largest annual changes of concentration in November and December were both +0.51 µg m^{-3}, while the smallest was for July (+0.23 µg m^{-3}). Seasonally, winter has the strongest upward trend (Q = 0.0117 µg m^{-3} $year^{-1}$; increase over the entire year = 0.47 µg m^{-3}), followed by autumn, spring, and summer in this order. Monthly distribution is characterized by a strong peak in the cold months (December and January) and a marked secondary peak in autumn (November). On the contrary, they are least concentrated during spring and summer. The greater standard deviations in winter and December denote episodic pollution peaks, while the similar, lower ones in spring and summer represent an immobile urban background. On the whole, the temporal evolution of BC shows a stable and statistically significant upward trend, with winter and autumn being the two dirtiest seasons.

A comprehensive study over the Arabian Peninsula using MERRA-2 reanalysis data (2000–2024) identified statistically significant positive trends in Black Carbon and surface air temperature over Kuwait and Riyadh (Shahid et al.,2026). The study demonstrated that BC peaks in summer due to combustion emissions and secondary aerosol formation. These findings align with our observed positive trends in Iraq (annual Q = 0.0060 µg m^{-3} yr^{-1}, $p < 0.001$), suggesting a coherent regional signal of deteriorating air quality across the Middle East driven by both natural dust processes and anthropogenic emissions.

Over Greater Cairo, Egypt, a study examining the seasonal and annual variability of BC and particulate matter from 2003 to 2020 found that winter had the highest concentrations, while summer had the lowest - a seasonal pattern consistent with our findings for Iraq. This suggests that the meteorological drivers of BC seasonality (stable atmospheric conditions and increased heating-related combustion in winter; enhanced vertical mixing in summer) operate similarly across the broader Middle East and North Africa region (Dawoud et al., 2023).

The spatial analysis of BC concentrations across Iraq shows a clear geographical gradient over the study period. BC concentrations in central and southern areas (e.g., Baghdad, Nasiriya, and Basra) consistently showed the highest values, with peaks (wintertime averages exceeding 1.8 µg m^{-3}). Conversely, no northern or westward areas observed concentrations higher than 0.2–1.0 µg m^{-3}. For all seasons, the first rank is occupied by the Zone center; after that, the southern and northern regions, with the western last. There are prominent spatial contrasts on a seasonal scale in winter (December–February) with central-south values >1.8 μg m^{-3}, and western locations dropping to 0.2–0.4 μg m^{-3}. Summer (June–August) has a uniform spatial distribution with central and southern concentrations of 0.6–1.0 μg m^{-3}, while western regions are between 0.2 and 0.6 μg m^{-3}. In autumn, spatial inequality also shows a second peak, with the southeastern cores exceeding 1.8 μg m^{-3}. The low levels in the western region reflect its arid, less urbanized nature. Spatially, BC pollution in Iraq is therefore not uniform but strongly localized, with the central-southern belt acting as a persistent pollution hotspot across all seasons.

References:

Adeeb, H. Q., & Al-Timimi, Y. K. (2019). GIS techniques for mapping of wind speed over Iraq. *Iraqi Journal of Agricultural Sciences*, 50(6). https://doi.org/10.36103/ijas.v50i6.852

Ahmed, T., Dutkiewicz, V. A., Khan, A. J., & Husain, L. (2014). Long-term trends in black carbon concentrations in the Northeastern United States. *Atmospheric Research*, 137, 49–57. https://doi.org/10.1016/j.atmosres.2013.10.003

Al-Jeelani, H. A. (2009). Evaluation of air quality in the Holy Makkah during Hajj season 1425 H. *Journal of Applied Sciences Research*, 5(1), 115–121.

Al-Lami, A. M., Al-Timimi, Y. K., & Al-Shamarti, H. K. (2021). Spatiotemporal analysis of some extreme rainfall indices over Iraq (1981–2017). *Scientific Review Engineering and Environmental Sciences*, *30*(2), 221-235.https://doi.org/10.22630/PNIKS.2021.30.2.19

Amann, M., Bertok, I., Borken-Kleefeld, J., Cofala, J., Heyes, C., Höglund-Isaksson, L., & Winiwarter, W. (2011). Cost-effective control of air quality and greenhouse gases in Europe: Modeling and policy applications. *Environmental Modelling & Software*, 26(12), 1489–1501. https://doi.org/10.1016/j.envsoft.2011.07.012

Atta, H. A. (2020). Assessment and geographic visualization of salinity of Tigris and Diyala Rivers in Baghdad City. *Environmental Technology & Innovation*, 17, 100538.https://doi.org/10.1016/j.eti.2019.100538

Becerril-Valle, M., Coz, E., Prévôt, A. S. H., Močnik, G., Pandis, S. N., de la Campa, A. S., & Artíñano, B. (2017). Characterization of atmospheric black carbon and co-pollutants in urban and rural areas of Spain. *Atmospheric Environment*, 169, 36–53. https://doi.org/10.1016/j.atmosenv.2017.09.014

Bian, Q., Alharbi, B., Shareef, M. M., Husain, T., Pasha, M. J., Atwood, S. A., & Kreidenweis, S. M. (2018). Sources of PM2.5 carbonaceous aerosol in Riyadh, Saudi Arabia. *Atmospheric Chemistry and Physics*, 18(6), 3969–3985. https://doi.org/10.5194/acp-18-3969-2018

Bond, T. C., Doherty, S. J., Fahey, D. W., Forster, P. M., Berntsen, T., DeAngelo, B. J., & Zender, C. S. (2013). Bounding the role of black carbon in the climate system: A scientific assessment. *Journal of Geophysical Research: Atmospheres*, 118(11), 5380–5552. https://doi.org/10.1002/jgrd.50171

CAPP. (2007). *Recommended Approach to Completing the National Pollutant Release Inventory (NPRI) for the Upstream Oil and Gas Industry*. Canadian Association of Petroleum Producers.

Chen, C., McCabe, D. C., Fleischman, L. E., & Cohan, D. S. (2022). Black carbon emissions and associated health impacts of gas flaring in the United States. *Atmosphere*, 13(3), 385. https://doi.org/10.3390/atmos13030385

Collaud Coen, M., Andrews, E., Bigi, A., Martucci, G., Romanens, G., Vogt, F., & Vuilleumier, L. (2020). Effects of the prewhitening method, the time granularity, and the time segmentation on the Mann–Kendall trend detection and the associated Sen's slope. *Atmospheric measurement techniques*, *13*(12), 6945-6964. https://doi.org/10.5194/amt-13-6945-2020

Conrad, B. M., & Johnson, M. R. (2017). Field measurements of black carbon yields from gas flaring. *Environmental Science & Technology*, 51(3), 1893–1900. https://doi.org/10.1021/acs.est.6b03690

Davuliene, L., Sakalys, J., Dudoitis, V., Reklaite, A., & Ulevicius, V. (2019). Long-term black carbon variation in the South-Eastern Baltic Region in 2008–2015. *Atmospheric Pollution Research*, 10(1), 123–133. https://doi.org/10.1016/j.apr.2018.06.013

Dawoud, W., El Kenawy, A. M., Abdel Wahab, M. M., & Oraby, A. H. (2023). Temporal variability of particulate matter and black carbon concentrations over Greater Cairo and its atmospheric drivers. *Climate*, *11*(7), 133. https://doi.org/10.3390/cli11070133

Ding, A. J., Huang, X., Nie, W., Sun, J. N., Kerminen, V. M., Petäjä, T., & Fu, C. B. (2016). Enhanced haze pollution by black carbon in megacities in China. *Geophysical Research Letters*, 43(6), 2873–2879. https://doi.org/10.1002/2016GL067745

Garnero, G., & Godone, D. (2014). Comparisons between different interpolation techniques. *International Archives of the Photogrammetry, Remote Sensing and Spatial Information Sciences*, 40, 139–144. https://doi.org/10.5194/isprsarchives-XL-5-W3-139-2013

Gilbert, R. O. (1987). *Statistical Methods for Environmental Pollution Monitoring*. Van Nostrand Reinhold.

Grieshop, A. P., Reynolds, C. C., Kandlikar, M., & Dowlatabadi, H. (2009). A black carbon mitigation wedge. *Nature Geoscience*, 2(8), 533–534. https://doi.org/10.1038/ngeo595

Hassan, S. F. (2018). *Modeling Infrastructure Maintenance Contracts in a Geospatial Database* [Master's thesis].

Hessl, A., Miller, J., Kernan, J., Keenum, D., & McKenzie, D. (2007). Mapping paleo fire boundaries from binary point data: comparing interpolation methods. *The Professional Geographer*, 59(1), 87–104. https://doi.org/10.1111/j.1467-9272.2007.00593.x

Huang, F., Liu, D., Tan, X., Wang, J., Chen, Y., & He, B. (2011). Explorations of the implementation of a parallel IDW interpolation algorithm in a Linux cluster-based parallel GIS. *Computers & Geosciences*, 37(4), 426–434. https://doi.org/10.1016/j.cageo.2010.08.001

Hyvärinen, A. P., Kolmonen, P., Kerminen, V. M., Virkkula, A., Leskinen, A., Komppula, M., & Lihavainen, H. (2011). Aerosol black carbon at five background measurement sites over Finland, a gateway to the Arctic. *Atmospheric Environment*, 45(24), 4042–4050. https://doi.org/10.1016/j.atmosenv.2011.04.026

IPCC. (2013). *Climate Change 2013: The Physical Science Basis*. Cambridge University Press.

Kouassi, A. A. (2021). Measurement of atmospheric black carbon concentration in rural and urban environments: cases of Lamto and Abidjan. *Journal of Environmental Protection*, 12(11), 855–872. https://doi.org/10.4236/jep.2021.1211050

Liu, G., Yan, Z., Wang, H., & Yang, Y. (2025). Visualization of the spatial transport of nutrients and organic matter contents in sediments under hydrodynamic perturbation conditions. *Science of The Total Environment*, 977, 179384. https://doi.org/10.1016/j.scitotenv.2025.179384

Lund, M. T., Berntsen, T. K., & Samset, B. H. (2017). Sensitivity of black carbon concentrations and climate impact to aging and scavenging in OsloCTM2–M7. *Atmospheric Chemistry and Physics*, 17(9), 6003–6022. https://doi.org/10.5194/acp-17-6003-2017

Muter, S. A., Al-Timimi, Y. K., & Al-Jiboori, M. H. (2024). Analysis of temporal and spatial drought characteristics in Iraq using the standard precipitation index (SPI). *IOP Conference Series: Earth and Environmental Science*, 1371(2), 022032. https://doi.org/10.1088/1755-1315/1371/2/022032

Nayebare, S. R., Aburizaiza, O. S., Siddique, A., Carpenter, D. O., Hussain, M. M., Zeb, J., & Khwaja, H. A. (2018). Ambient air quality in the holy city of Makkah: A source apportionment with elemental enrichment factors (EFs) and factor analysis (PMF). *Environmental Pollution*, 243, 1791–1801. https://doi.org/10.1016/j.envpol.2018.09.086

Raju, M. P., Safai, P. D., Vijayakumar, K., Devara, P. C. S., Naidu, C. V., Rao, P. S. P., & Pandithurai, G. (2016). Atmospheric abundances of black carbon aerosols and their radiative impact over an urban and a rural site in SW India. *Atmospheric Environment*, 125, 429–436. https://doi.org/10.1016/j.atmosenv.2015.09.023

Reimann, C., Filzmoser, P., Garrett, R., & Dutter, R. (2011). *Statistical Data Analysis Explained: Applied Environmental Statistics with R*. John Wiley & Sons.

Robinson, T. P., & Metternicht, G. (2003). A comparison of inverse distance weighting and ordinary kriging for characterizing within-paddock spatial variability of soil properties in Western Australia. *Cartography*, 32(1), 11–24. https://doi.org/10.1088/00690805.2003.9714231

Sadar, M. W., Al-Jiboori, M. H., & Al-Timimi, Y. K. (2023). Spatial Analysis of PM2.5 Concentration over Iraq during 2003-2020. *Journal of the Earth and Space Physics*, 48(4).http//doi.org/10.22059/jesphys.2022.344671.1007441

Samset, B. H., Myhre, G., Schulz, M., Balkanski, Y., Bauer, S., Berntsen, T. K., & Zhang, K. (2013). Black carbon vertical profiles strongly affect its radiative forcing uncertainty. *Atmospheric Chemistry and Physics*, 13(5), 2423–2434. https://doi.org/10.5194/acp-13-2423-2013

Samudro, H., Samudro, G., & Mangkoedihardjo, S. (2023). Cleaning up black carbon using plant strategies. *Plant Science Today*, 10(2), 310–315. https://doi.org/10.14719/pst.2179

Sánka, O. (2015). *Use of Geographic Information Systems in Environmental Science* [PhD thesis]. Masarykova Univerzita.

Shahid, I., Ullah, M. I., Javed, S., Shahzad, M. I., Mahfouz, M. M., Tutsak, E., & Umar, M. (2026). Spatiotemporal Variability, Trends, and Projected Evolution of Aerosols over the Arabian Peninsula. Earth Systems and Environment, 1-21. https://doi.org/10.1007/s41748-026-01216-1

Weyant, C. L., Shepson, P. B., Subramanian, R., Cambaliza, M. O., Heimburger, A., McCabe, D., & Bond, T. C. (2016). Black carbon emissions from associated natural gas flaring. Environmental science & technology, 50(4), 2075-2081. https://doi.org/10.1021/acs.est.5b04712

Wahab, B. I., Hassan, B. J., Al-Timimi, Y. K., & Al-Ataby, I. K. (2023). Relationship between the concentrations of black carbon and some meteorological parameters over Iraq using GIS techniques. *IOP Conference Series: Earth and Environmental Science*, 1223(1), 012015. https://doi.org/10.1088/1755-1315/1223/1/012015

Zangana, L. M., Al-Temimi, B. I. W., & Aljuhaishi, S. A. (2021). Analytical study of rate volume liquid water content in low clouds over Iraq. *Iraqi Journal of Agricultural Sciences*, 52(4), 783–792.https://doi.org/10.36103/ijas.v52i4.1387

Zhang, H., & Wang, Z. (2011). Advances in the study of black carbon effects on climate. *Advances in Climate Change Research*, 2(1), 23–30.https://doi.org/10.3724/SP.J.1248.2011.00023

Zhang, X., Li, L., Che, H., Dubovik, O., Derimian, Y., Holben, B., ... & Zhang, X. (2024). Aerosol components derived from global AERONET measurements by GRASP: a new value-added aerosol component global dataset and its application. Bulletin of the American Meteorological Society, 105(10), E1822-E1848.https://doi.org/10.1175/BAMS-D-23-0260.1

Zhang, Y., Li, Y., Guo, J., Wang, Y., Chen, D., & Chen, H. (2019). Climatology and trends of black carbon in China from 12-year ground observations. *Climate Dynamics*, 53, 5881–5892. https://doi.org/10.1007/s00382-019-04903-0